16TH EUROPEAN CONFERENCE ON EARTHQUAKE ENGINEERING THESSALONIKI 18 - 21 JUNE 2018

DAMAGE ASSESSMENT FOR BURIED PIPES AFFECTED BY GROUND MOTIONS AND LIQUEFACTION IN THE 2011 OFF THE PACIFIC COAST OF TOHOKU EARTHQUAKE

Gaku SHOJI[1], Reina KOBAYASHI[2], Masahiro HARA[3]

ABSTRACT

This study examined the dependence of damage of buried pipes used for water supply systems and sewer systems in the 2011 off the Pacific coast of Tohoku earthquake on the strong motion intensities obtained for liquefied and non-liquefied grounds at Kamisu City in Ibaraki Prefecture, Japan. The relations between the damage ratio and the ground motion intensities were reasonably explained by classifying the targeted sites by the soil properties. The modeling of associated fragility curves were also attempted with respect to the peak ground velocity by classifying the value of potential liquefaction for the targeted sites

Keywords: Buried pipe; Seismic damage; the 2011 off the Pacific coast of Tohoku earthquake; Liquefaction; Effective stress analysis

1. INTRODUCTION

The earthquake off the Pacific coast of Tohoku on March 11th, 2011 (hereinafter referred to as "the Tohoku earthquake") caused major damage to water supply systems and sewerage systems. According to the Ministry of Health, Labor and Welfare (2013), water outages occurred at a maximum of 2,567,210 houses in 21 prefectures and Tokyo Metropolitan. Additionally, the Ibaraki Prefecture included the maximum number of water outage houses (801,018 houses). Sewerage disruption outages also occurred in 10 prefectures and Tokyo. The Sewerage Technological Examination Committee for Earthquake and Tsunami (2016) indicated that the damaged length of sewer pipes corresponded to 642 km for the total length of the buried sewer pipes (65,001km).

Prior to the Tohoku earthquake, several researchers discussed seismic reliability of water supply systems and sewerage systems (for example, Hwang *et al*. (1998), Liu & Hung (2009), Javanbarg & Takada (2009), Shoji *et al*. (2011)). Following the Tohoku earthquake, researchers evaluated damages on water supply and sewage systems by various indices of ground motion intensity (for example, Naba *et al*. (2012), Toprak *et al*. (2017)). Tsukiji and Shoji (2013) analyzed the dependence of damage ratio of buried distribution pipes on the spatial distribution of peak ground velocity (*PGV*) at Itako City and Kamisu City in the Ibaraki Prefecture, Japan and derived the associated fragility curves. However, these studies did not focus on site-specific ground motions and liquefaction at the target sites. Detailed analyses under the ground are required to clarify the dependence of pipe damage on ground motion intensity. Unjoh *et al*. (2013) investigated the effect of seismic ground motions on soil liquefaction by performing a one-dimensional soil response analysis. We follow the same and provide more detailed considerations for the dependence of the pipe damage on the ground motion.

The purpose of this study involves analyzing the damage to buried pipes by considering the mechanical properties of the ground. First, we model the soil layers at 39 target sites based on the data from boring

[1]Associate Prof., Dr.Eng., University of Tsukuba, Tsukuba, Japan, gshoji@kz.tsukuba.ac.jp

[2]Graduate Student, Graduate School of Systems and Information Eng., University of Tsukuba, Tsukuba, Japan, s1720935@s.tsukuba.ac.jp

[3]Ditto, s1620916@u.tsukuba.ac.jp

surveys and associated soil tests. Second, we perform the one-dimensional soil response analysis with the simplified effective stress method "YUSAYUSA" proposed by Yoshida and Towhata (1991). Subsequently, we reveal the dependence of damage ratio of pipes and ground motion intensity and liquefaction. Finally, we develop more precise fragility curves that reflect the dependence when compared to previous fragility curves by classifying the target sites based on the mechanical properties of the ground.

2. SOIL RESPONSE ANALYSIS AT DAMAGED SITE

2.1 Subject area

The subject area is the northern-west part in Kamisu City, Ibaraki Prefecture. Figure 1 shows the water supply and the sewer system networks in Kamisu City in which buried pipes were severely damaged by the liquefaction in the 2011 Tohoku earthquake. We examined a total of 39 target sites: 33 sites were liquefied and the other 6 sites were non-liquefied. The liquefaction area was defined based on data from Tsukiji and Shoji (2013), which were originally from by Japanese Geotechnical Society and The Kanto District Bureau of MILT (reported as the Kanto District Bureau of MILT (2011)).

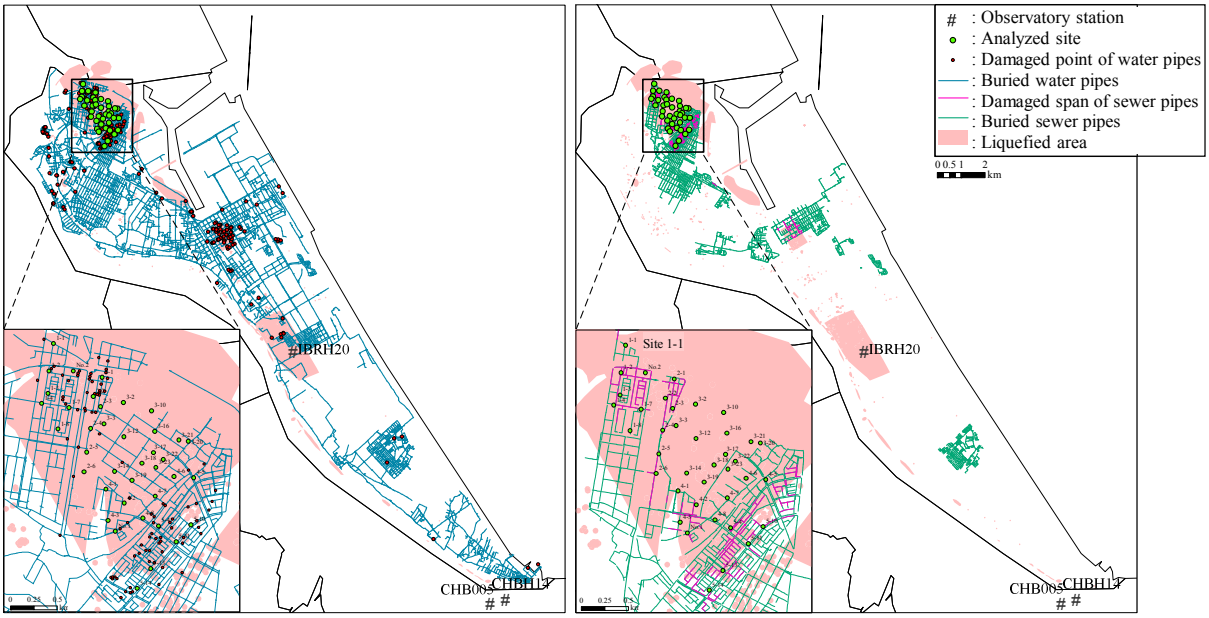

Figure 1 Buried pipe networks in the subject area

2.2 Modeling Method of Soil layers for Analysis

For each site, a set of soil layers with a total depth from 15.5 m to 26.6 m were modeled one-dimensionally and elastically by multi-degree of freedom systems with mass spring and dashpot as shown in Figure 2. In terms of the boundary condition at the bottom, the radiation damping effect was considered, and the bottom layer and base layer were linked with dashes. We used the data of geologic columnar sections, the depth of ground water level, and the result of standard penetration tests.

We idealized the soil layers from 8 layers to 9 layers. We divided the layers referring to soil classification, ground water level, and *N*-value. First, we categorized them into layers above or below the ground water level. Second, when several layers have the same soil property range but their *N*-values differ along the depth, then we defined the boundary based on the *N*-value. Each of the layer thickness ranged from 0.3 m to approximately 3.6m.

The parameters were set as follows. The average *N*-value at the *i*-th layer was calculated by linearly interpolating the *N*-value data by standard penetration tests. Liquefaction strength ratio is determined as the cyclic stress ratio R_L, which raises reversed amplitude strain to 5% in 20 cycles. If a layer was not

tested for liquefaction strength, R_L was spatially interpolated by the Bridge Design Specifications (2012).

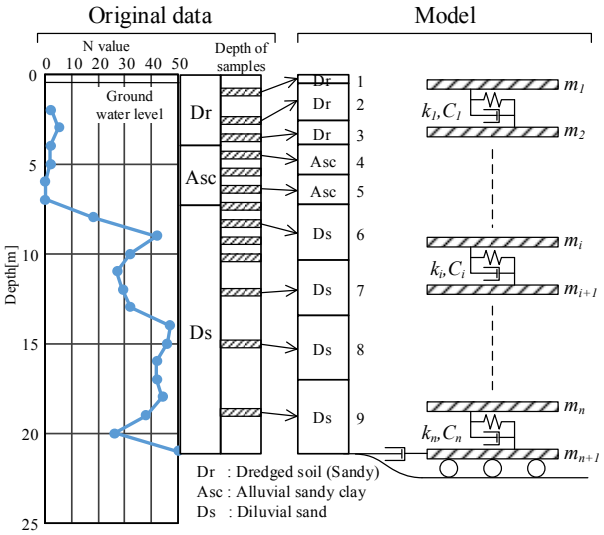

Figure 2 Soil layers model for site 1-1

Initial modulus of rigidity G_0 was calculated by Equation (1) as follows:

$$G_0 = \frac{\gamma_t {V_s}^2}{g} \tag{1}$$

where γ_t denotes unit weight of soil, and g denotes gravity acceleration. If shear modulus wave velocity V_s was unknown, it was estimated by applying the equations based on Bridge Design Specifications (2012) with use of N_i denoting the average of N-value at the i-th layer. Internal frictional angle φ for i-th layer was set by the equations by Hatanaka and Uchida (1996). Coefficient of permeability k was set by Darcy's rule. It was estimated from the table given by Creager *et al*. (1945). In the analysis, we used Equation (2) based on the table as follows:

$$k = 0.0034{D_{20}}^{2.2954} \ (0.005 \le D_{20} \le 2) \tag{2}$$

If there was no value of D_{20} since the value was excessively low for measurement, we assumed that D_{20} corresponds to 0.02. With respect to the site that did not possess sufficient data for the standard penetration test and soil test, we used the data of nearby sites in which soil classification is similar.

2.3 Method and Condition of Analysis

We performed a one-dimensional effective stress analysis by using the computer program YUSAYUSA-2 developed by Yoshida and Towhata (1991). With respect to the shear stress τ-strain γ model, we used Hardin-Drnevich model. The hysteresis curve obeys Masing rule. The increase in pore water pressure was calculated by the effective stress path proposed by Ishihara and Towhata (1980). The equation of motion was solved by Newmark's β scheme with $\beta = 0.25$. Permeability was calculated by the following equations that depict the vertical movement of soil particle and water following Biot's method as follows:

$$\frac{\gamma_t}{g}\frac{\partial W}{\partial t} + \frac{\gamma_w}{g}\frac{\partial Q}{\partial t} = -\frac{\partial \sigma}{\partial z} + \gamma_t \tag{3a}$$

$$\frac{n\gamma_w}{g}\frac{\partial W}{\partial t} + \frac{\gamma_w}{g}\frac{\partial Q}{\partial t} + \frac{b}{n}Q + n\frac{\partial u}{\partial z} - n\gamma_w = 0 \tag{3b}$$

$$\frac{\partial W}{\partial z} + \frac{\partial Q}{\partial z} = 0 \tag{3c}$$

$$\frac{\partial W}{\partial z} = m_v \left(-\frac{\partial \sigma}{\partial t} + \frac{\partial u}{\partial t} - \frac{\partial u_g}{\partial t} \right) \tag{3d}$$

where W denotes downward velocity of soil particle, Q denotes relative velocity of pore water with soil particles, σ denotes the total stress, u denotes effective water stress, u_g denotes excess pore water pressure, γ_t denotes the unit weight of soil, γ_w denotes the unit weight of water, n denotes porosity, k denotes the coefficient of permeability, b is equal to $n^2\gamma_w/k$, and m_v denotes the coefficient of volume compressibility. These equations were solved by using the Galerkin method. The boundary condition in the permeability equation was set as W=0 (imperviousness) at the ground water level and base ground surface. The ground water level was fixed.

The series of the analyses were conducted in both EW and NS directions. In this study, we focused on the results in the EW direction because the ground motions in the EW direction exceeded those in the NS direction. Excess pore water pressure ratio is defined as excess pore water pressure u_e divided by initial loading pressure σ_{v0}'. The upper limit of excess pore water pressure ratio u_e/σ_{v0}' is 0.97, and this was used as the criteria of liquefaction occurrences. The time increment is 0.01 s and the time duration is 300 s.

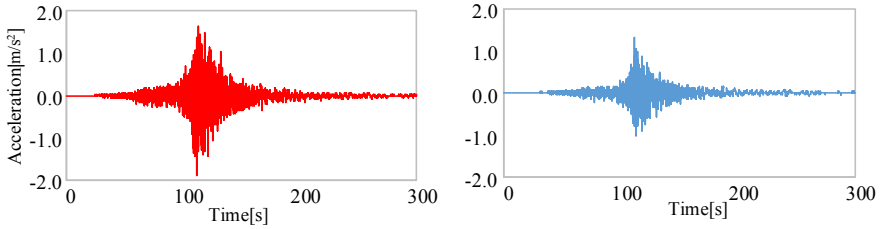

(a) Wave form observed at the ground surface (b) Calculated wave form at the basement

Figure 3. Input wave (IBRH20, EW direction)

Input seismic waves to engineering bedrock with Vs = 350 m/s were presumed by the equivalent linear method with the acceleration wave form observed at IBRH20, which is one of KiK-net stations near the subject area. Based on the soil profile at IBRH20, we separated the soil layers into 31 layers in a unit of 2.0 m thickness and calculated input wave by using the ground response analysis program DYNEQ (Yoshida and Suetomi (1988)). Figure 3(a) shows the observed wave in the EW direction at the surface on IBRH20, and Figure 3(b) shows the calculated wave in the EW direction at the engineering bedrock.

3. DEPENDENCE OF DAMAGE ON GROUND MOTION AND LIQUEFACTION

3.1 Result of Ground Response Analysis

Figure 4 shows the examples of the analysis results. Table 1 shows the characteristics of the sites. Figure 4(a) depicts the results for the 2nd layer at site 1-1 that was liquefied in the analysis and the actual field survey performed by Japanese Geotechnical Society and the Kanto District Bureau of MILT. Typical liquefaction was recognized. Figure 4(b) shows the result for the 3rd layer at site 4-2 that was not liquefied in the analysis but was actually liquefied. Figure 4(c) shows the result at the 6th layer at site 5-10 that was identified as liquefied in both the analysis and the field survey. The liquefaction occurred in the lower layers from 6 m to 10 m at the site.

Table 1. Comparison of the results and estimations

Site number	Field survey	Estimation with *FL*	Effective stress analysis
1-1	Liquefied	Dangerous	Liquefied
4-2	Liquefied	Dangerous	Not liquefied
5-10	Liquefied	Dangerous	Liquefied

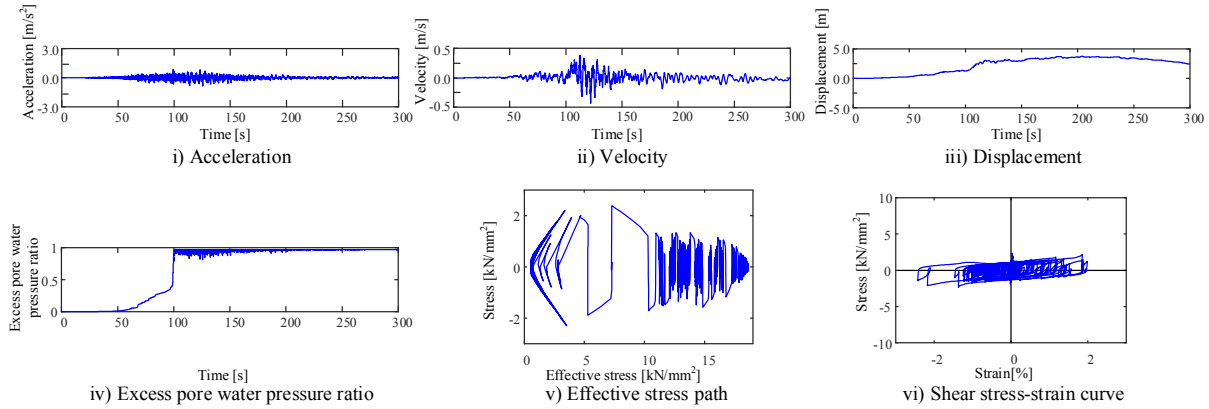

(a) 2nd layer at site 1-1 (EW direction)

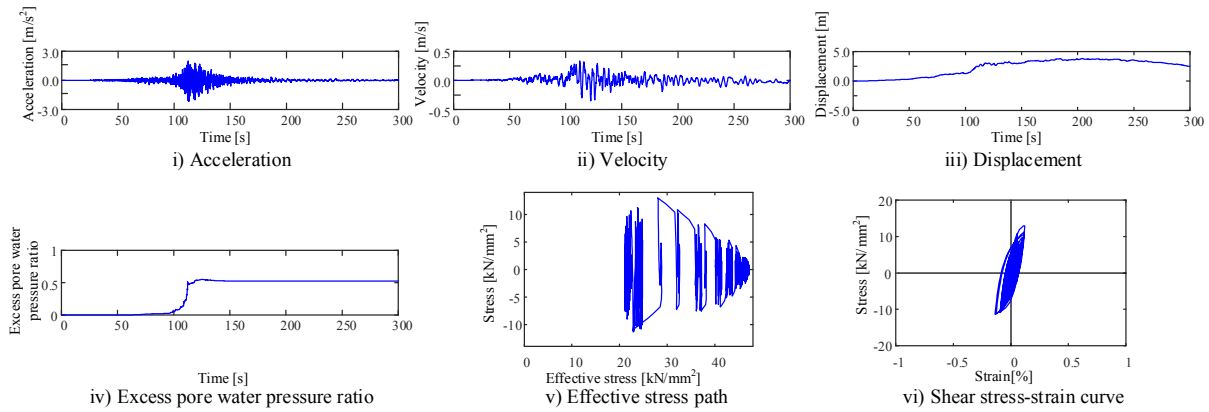

(b) 3rd layer at site 4-2 (EW direction)

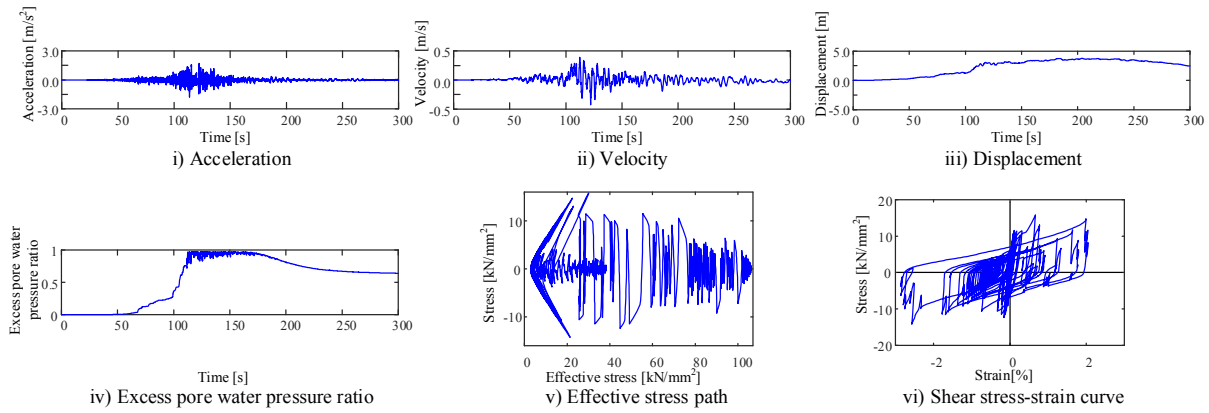

(c) 6th layer at site 5-10 (EW direction)

Figure 4. Time history responses

From Figure 4(a), at the site 1-1, the time involved corresponded to 33 s when the excess pore water pressure ratio varied from 0.1 to 0.97. The displacement started to increase after the occurrence of the liquefaction. The residual displacement at 300 s was 2.49 m. The maximum shear strain reached 2.43%. The maximum acceleration was 0.83 m/s^2 and the maximum velocity was 0.33 m/s. When compared with site 1-1, the excess pore water pressure ratio rose from 105 s to 125 s at the site 4-2 as shown in Figure 4(b) although it stopped at approximately 0.5 and did not reach 0.97. The residual displacement was 2.45 m, and this is the same level as that at site 1-1. The stress-strain relationship exhibited slightly non-linear behavior around the elastic range. The maximum shear strain was 0.138%, and this was less than 0.2% and smaller than that of site 1-1. The maximum value of acceleration was 1.96 m/s^2, and this is approximately twice that of site 1-1. Conversely, the time history of velocity basically exhibited the same trend as that of site 1-1. The maximum velocity was 0.38 m/s, and this is nearly equal to site 1-1. At site 5-10 as shown in Figure 4(c), the excess pore water pressure ratio increased from 70.7 s to 113.8 s, and it reached the upper limit of 0.97. Subsequently, it started to decline at 173.2 s and reached 0.64

at 300 s. We recognized the dissipation at the lower layers although it did not occur at the upper layers. The period of increase in the excess pore water pressure ratio at site 5-10 exceeded that of site 1-1 by 10 s, and thus the total period corresponded to 60 s. The residual displacement was 2.47 m. The stress-strain relationship evidently demonstrated the non-linear behavior. The ground was obviously non-linearized and the maximum shear strain was 2.86%. The maximum value of acceleration was 1.72 m/s^2 and the maximum value of velocity was 0.39 m/s. In terms of the wave shape and value range, the displacements and velocity of these three sites were similar to each other although the accelerations were different.

Figure 5 depicts the comparison of liquefied layers on the analysis and the prediction of liquefaction based on resistance coefficient for liquefaction, *FL*. Specifically, *FL* is defined by Equation (4). In this study, we referred to the Recommendations for Design of Building Foundations (1988), and *FL* was calculated at depths of l.0 m each. The anticipated ground motion was set as earthquake magnitude of *M*=9.0 and *PGA*=2.0 m/s. The expression is as follows:

$$FL = \frac{R}{L} \tag{4}$$

where *R* denotes liquefaction strength, and *L* denotes cyclic shear strength. The layer with $FL \leq 1.0$ is considered as it is liquefied.

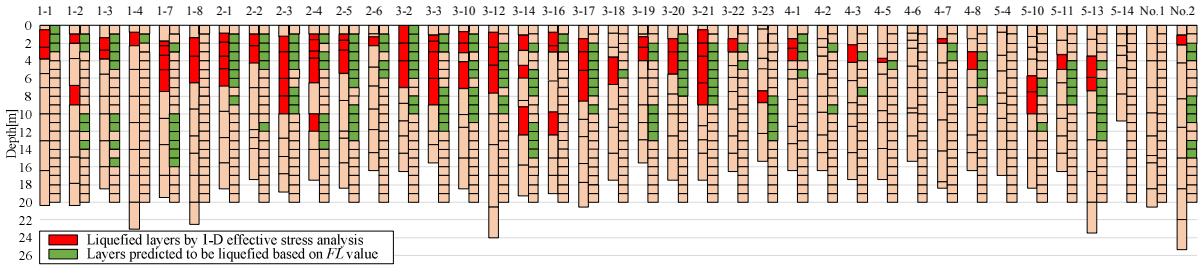

Figure 5. Results of one-dimensional effective stress analysis

According to Figure 5, 33 target sites exhibited the same judgments about the occurrence of liquefaction by the analysis and in Figure 1. In contrast, the results at 6 target sites (i.e., sites 4-2, 4-5, 4-7, 4-8, 5-11, and No. 1) corresponded to the field survey results. With respect to sites 4-2, 5-11, and No.1, we assume that the reason for the difference is a margin of error by the linear interpolation of average *N*-value for modeling the objective soil layers. With respect to sites 4-5 and 4-7, we are also sure that a few liquefied layers in the target sites were excessively thin (less than 0.5 m thick) to observe the liquefaction damage. Site 4-8 is on the edge of the non-liquefied area. It might be considered as liquefied.

In terms of the *FL*-value prediction, the results of the analysis generally agree with the prediction in terms of depth and thickness of liquefied layers above a depth of 10 m. At sites 1-3, 2-5, 3-12, No.2, and the eleven other sites, the prediction under a depth of 9.0 m showed that the sites liquefy although the analysis did not predict the same. This is because the influence of permeability was not considered during the process of calculating *FL*. Therefore, the results of the analysis are more appropriate than those of the prediction.

3.2 Definition of Damage Ratio and Evaluation Scheme

3.2.1 Definition of Damage Ratio

We quantified damage of water distribution pipes and sewer pipes as defined by following Equations (5a) and (5b). Damage ratio of water supply system is R_w [point/km] and the one of sewer system is R_s [km/km] as follows:

$$R_w = \frac{N_{dw}}{L_{bw}} \tag{5a}$$

$$R_s = \frac{L_{ds}}{L_{bs}} \tag{5b}$$

where, the number of physical damage points of distribution pipes is denoted as N_{dw}, the total lengths of distribution pipes is L_{bw} [km], lengths of damaged sewer pipes is L_{ds} [km], and total lengths of sewer pipes is L_{bs} [km].
The objective areas to calculate damage ratio were within 100 m in radius from each analyzed site. If the distributed pipe length was less than 200 m in each area, then the associated data was removed.
The estimated buried depths of pipes were determined by previous interviews conducted with the water supply and sewerage department of Kamisu City. When we discuss the damage of buried pipes, the estimated buried depth of water pipes is 1m and that of sewer pipes is 3 m.

3.2.2 Indices for Damage Analysis

Table 2 and Table 3 show the indices for damage analysis. Indices in Table 2 shows the parameters of soil properties. They include media information inducing ground excitation. Table 3 lists the indices that show the strength of disturbance by seismic ground motions and liquefaction.

Table 2. Soil property indices

Index	Target system
Ground water level *GWL* [m]	WSS and SS
Average *N*-value (1m depth) N_1	WSS
Average *N*-value (3m depth) N_3	SS
PL-value *PL*	WSS and SS

WSS denotes water supply system and SS denotes sewerage system.

Table 3. Indices of ground motion and deformation

Index	Target system
Peak ground velocity *PGV* [m/s]	WSS and SS
Summation of thickness of liquefied layer H_L [m]	WSS and SS
Maximum shear strain γ_{max}	WSS and SS

WSS denotes water supply system and SS denotes sewerage system.

In Table 2, the average *N*-values N_1 and N_3 are at depths of 1.0 m and 3.0 m, respectively. The *PL* was proposed by Iwasaki et al. (1980). It indicates potential of liquefaction and it is originally identified by following equations:

$$PL = \int_0^{20} F \cdot w(z)dz \tag{6}$$

$$F = \begin{cases} 1 - FL & (FL < 1) \\ 0 & (FL \geq 1) \end{cases} \tag{7a}$$

$$w(z) = 10 - 0.5z \tag{7b}$$

where z denotes depth [m]. We change the interval of integration from 0.0 m to 10.0 m in Equation (6) and revise the weight $w(z)$ in Equation (7b) to be $w(z)$=20-2z because the depths of buried pipes are shallower than those of a large structure foundation. In Table 3, peak ground velocity *PGV* is calculated by vector composing along the EW and NS directions, and maximum shear strain γ_{max} is identified as the higher of the two values, namely the maximum in the EW direction or in NS direction. The thickness of liquefied layers H_L is the summation of the thickness of the liquefied layers.

3.3 Dependency of Damage on Soil Properties

Figure 6 shows that relation between damage ratio of buried pipes and soil properties. We investigated the dominant factor of the damage degree of buried pipes from the indices in Table 2. We selected the indices for use in the classification of target sites.

Figure 6(a) shows that only at the sites with $GWL \leq 1.5$ m, R_w exceeded 4.0 point/km and R_s exceeded 0.5 km/km. The damages were caused by the typical liquefaction in the upper layers. In contrast, sites 5-10 and 5-13 indicated high damage ratios among the sites with $GWL \geq 1.5$ m where R_w exceeded 1.7 point/km and R_s exceeded 0.28. As shown in Figure 5, liquefaction occurred at a depth lower than 3.0 m at these sites. This suggests that liquefaction in the deeper part of ground caused damage to the buried pipes. Figure 6(b) shows that the sites with $R_w \geq 4.0$ were $N_1 \leq 5.0$ with the exception of site No.2 and the sites with $R_s \geq 0.50$ are $N_3 \leq 7.0$. Specifically, with respect to sewer pipes, there were the data of $0.30 \leq R_s < 0.50$ at 8 sites with or without liquefaction although the surface ground was stiff since $N_3 > 12$. Figure 6(c) shows that PL at the target sites varied from 0 to approximately 40. The dependence of R_w or R_s on PL was not clear. However, with respect to R_w, all the sites with $R_w \geq 4.0$ point/km were with $PL \geq 15$ with the exception of site No.2. The damage ratio tended to be high at the sites with $PL \geq 15$. From the 14 sites with $PL > 15$, four sites belonged to $R_s \geq 0.80$ although five sites belonged to $R_s = 0$. The buried pipes are not necessarily damaged if liquefaction occurs. In contrast, only four out of 15 sites with $0.0 < R_s \leq 0.50$ belonged to $PL > 15$. For the reasons previously described, these indices categorized the degree of damage of pipes. Specifically, they could explain the damage with respect to higher R_w and R_s.

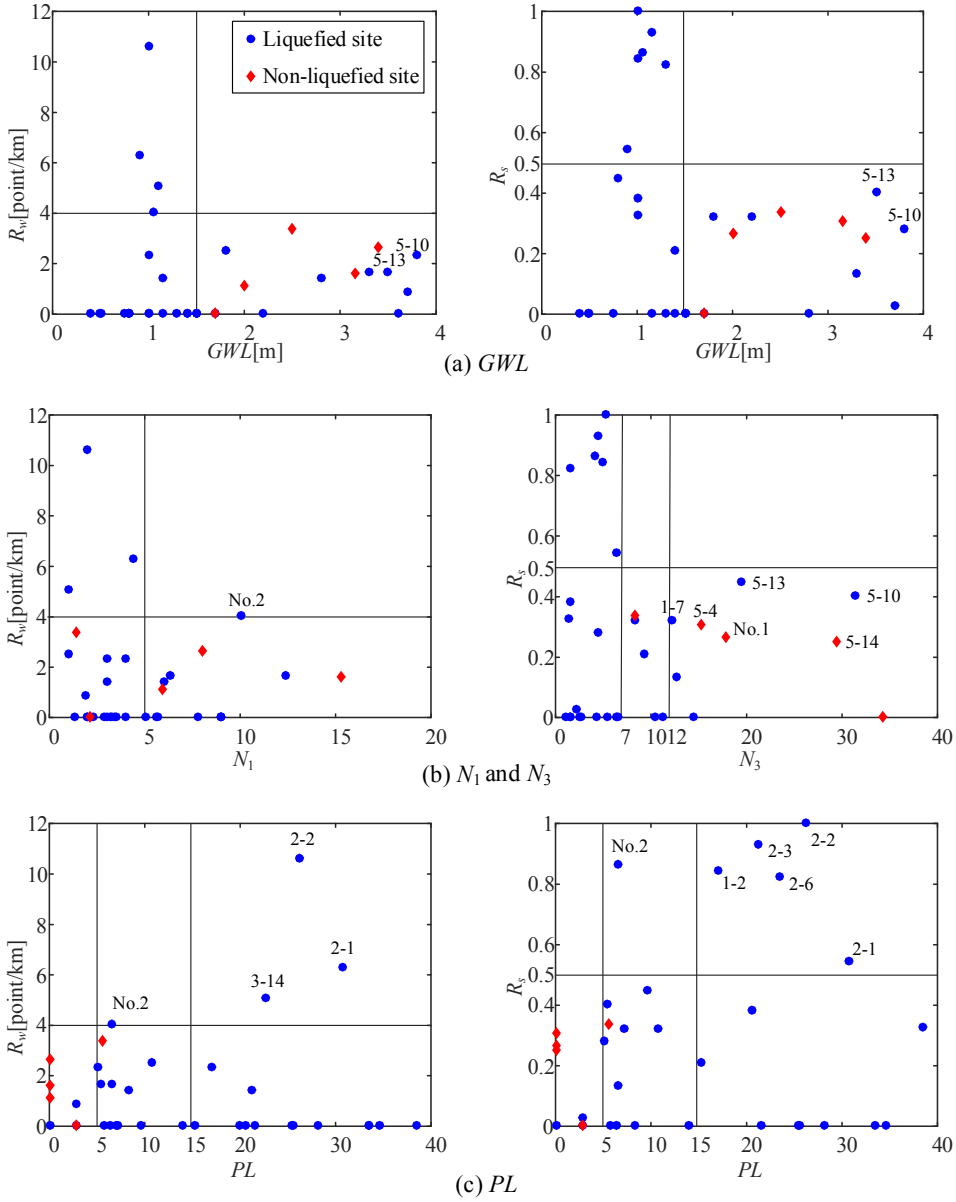

Figure 6. Relation between damage ratio and GWL, N_1 and N_3, or PL

3.4 Dependence of Damage on Ground Motions and Ground Deformation

Figure 7 shows the relation between the damage ratio of buried pipes and ground motion intensity or ground deformation. We investigated the factor of the damage degree of buried pipes with the indices listed in Table 3.

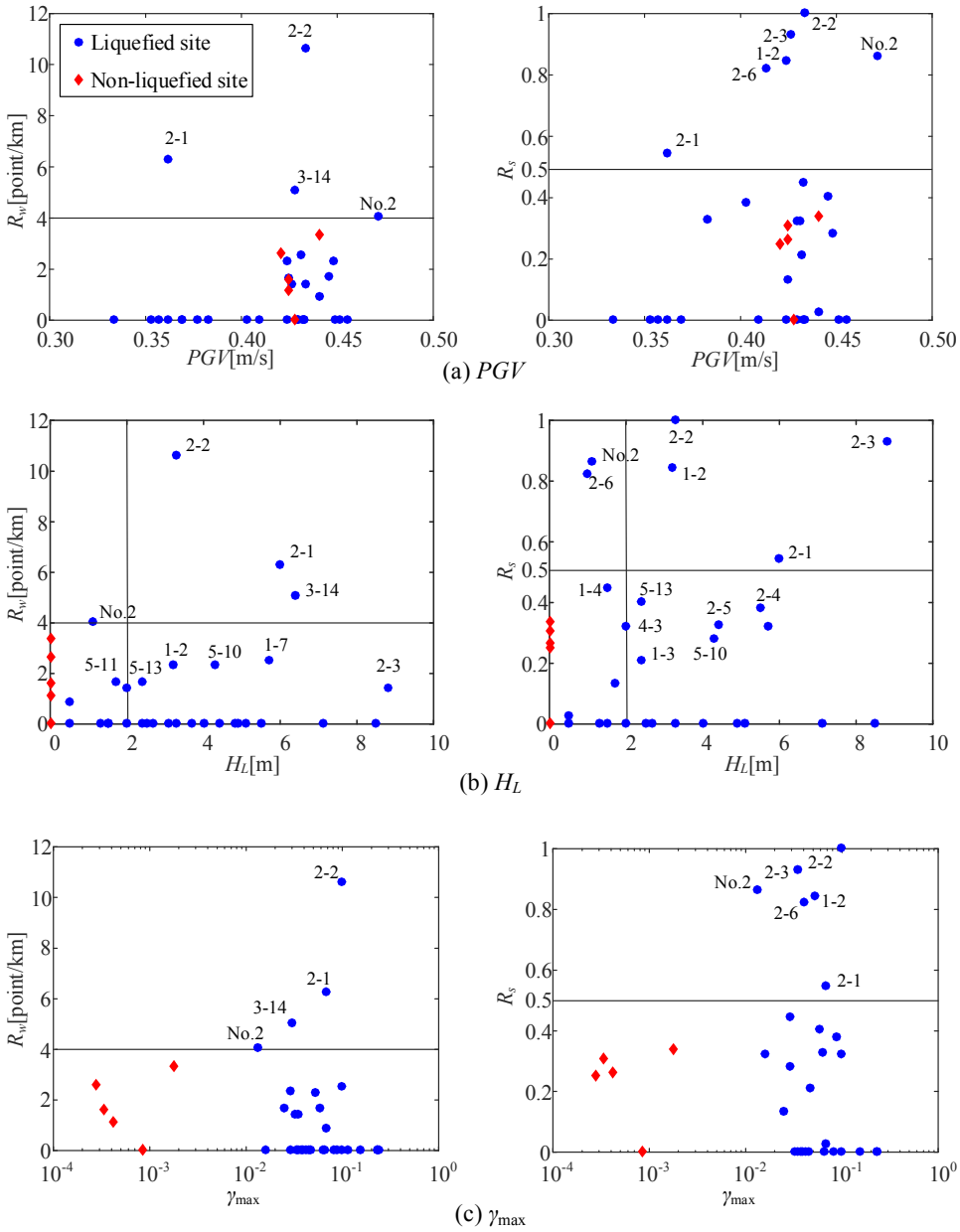

Figure 7. Relation between damage ratio and PGV, H_L, and γ_{max}

In Figure 7(a), with respect to the sites with $R_w \leq 4.0$ point/km, R_w began to increase from $PGV = 0.35$ m/s. However, the range of PGV at the four sites with $R_w \geq 4.0$ point/km was 0.36 m/s $\leq PGV \leq$ 0.47 m/s; and this was considered as wide range. In terms of the relation between PGV and R_s, R_s increased with increases in PGV in the range since $PGV > 0.35$ m/s. Figure 7(b) shows that the sites with $H_L \geq 2.0$ m suffered pipe damage in both the water supply and sewerage systems. Given the sites with $H_L \geq 2.0$ m, the sites with higher R_w or R_s, such as site 2-1, 2-2, and 3-14, were liquefied from the upper to the lower layers. Conversely, the sites with $H_L < 2.0$ m were liquefied only at the upper layers and were severely damaged. When compared with these, the sites only liquefied at the lower layers were included the damage range as $R_w < 4.0$ point/km or $R_s < 0.5$. This result implied that the liquefaction at the layers with buried pipes caused damage and that it might be difficult for liquefaction at lower layers to cause

the pipe damage from a depth of 1 m to 3 m. Furthermore, high H_L caused the damage of buried pipes. However, at the sites with high H_L, the ground motions reached a certain of the limit value and the damage by the ground motion was saturated. As a result, the depth of the liquefied layer is a better factor of R_w and R_s when compared to H_L. Figure 7(c) shows that R_w increased with increases in γ_{max} at the sites with $R_w \geq 4.0$ point/km while the sites with $R_w < 4.0$ point/km exhibited the scattering of γ_{max}. The liquefaction occurred in the upper layers at the former sites in contrast to the liquefaction of lower layers at the latter sites. When compared with R_w, R_s remained stable with increases in γ_{max} although the values were high. The results suggested that the ground deformation by liquefaction in upper layers could directly cause pipe damage and that the liquefaction in lower layers could also cause the half degree of damage.

4. MODIFICATION OF PREVIOUS FRAGILITY CURVES

First, we classified the actual data on damage ratios R_w and R_s at the target sites into two categories according to the *PL*-values described in the previous chapter, which threshold value is set as $PL = 15$. Second, we modeled the fragility curves describing the estimating value of damage ratios R_w and R_s by statistically analyzing the actual damage ratio data based on the cumulative distribution function of the log-normal distribution as shown in Equation (8) as follows:

$$R(PGV) = C\Phi\left(\frac{\ln(PGV) - \lambda}{\zeta}\right) \tag{8}$$

where Φ denotes the standard normal cumulative distribution function; C, λ, and ζ denote model parameters determined by using least square method minimizing objective function ε^m as described in the following equation. Now, C denotes the asymptotic value describing the limit of estimated damage ratio, λ and ζ are the expected value and the standard deviation of logarithmic value of *PGV*.

$$\varepsilon^m = \sum_{j=1}^{n_{PGV}} (R(PGV) - R_X(PGV))^2 L_j \tag{9}$$

where j denotes the number of classes of *PGV* in a 3 cm/s unit; n_{PGV} denotes the total number of *PGV* classes; R_X denotes the actual damage ratio R_w or R_s; and L_j denotes the length of exposed pipes for the j-th class in a 3 cm/s unit.

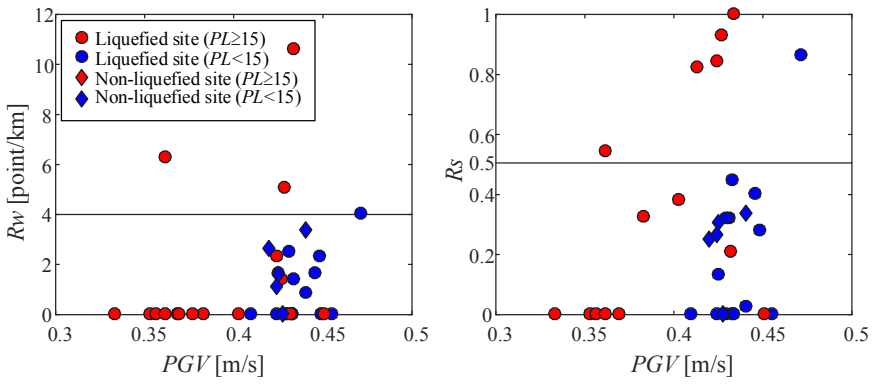

(a) Water pipes (b) Sewer pipes

Figure 8. Relation between the damage ratio and *PGV*

As shown in Figure 8, the $PL \geq 15$ group exhibited a lower *PGV* when compared to that of the $PL < 15$ group. When the threshold value was set as PL=15, it was effective to examine the difference of the pipe damage due to the ground conditions. Figure 8(a) shows that *PGV* and R_w were basically related to positive correlation for $PL < 15$ in the range of $PGV \geq 0.35$ m/s. The three points with the highest R_w

were in the group of $PL \geq 15$. Figure 8(b) shows that five sites were in the $PL \geq 15$ group and only one site was in the $PL < 15$ group given the sites with $R_s > 0.5$.

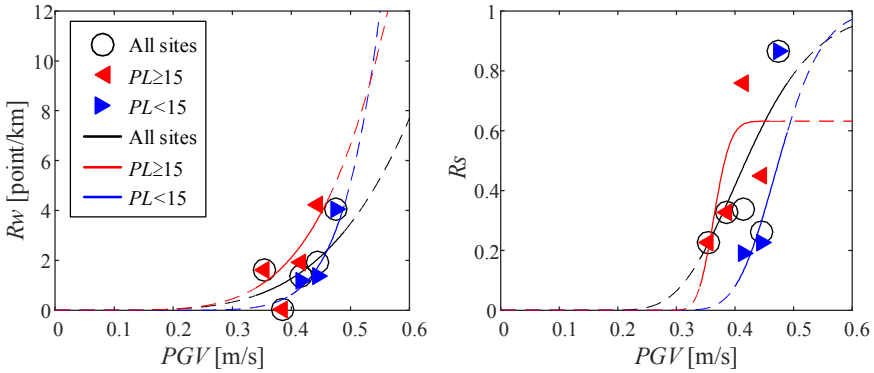

(a) Water pipes (b) Sewer pipes

Figure 9. Data of damage ratio and fragility curves

Figure 9 shows the fragility curves with the threshold value corresponding to $PL = 15$. The effective range is denoted by solid lines. The result suggests that it is possible to underestimate the damage ratio with a fragility curve that does not include the *PL*-value information. The fragility curves of both of two groups increase more sharply than those in all sites.

5. CONCLUSIONS

This study examined the dependence of damage of buried pipes on strong motion data in the 2011 Tohoku earthquake obtained for liquefied and non-liquefied grounds. The relations between the damage ratio and the ground motion intensities were classified by the soil properties. The modeling of fragility curves were also attempted with respect to the *PGV* and *PL*-values. The results are summarized as follows:

1) The numerical results from the one-dimensional effective stress analysis for 39 soil profiles at Kamisu City in Ibaraki Prefecture, Japan were in agreement with actual liquefaction and evaluation by using the *FL*-value. Liquefaction was observed mostly at lower layers in the analysis. However, it was not actually observed at the sites in which only the lower layers were liquefied

2) By observing the relations between R_w or R_s and *GWL*, N_1, N_3, or *PL*, these indices categorized the degree of damage of pipes with a few threshold values and they could explain the damage for higher R_w and R_s values.

3) From the relations between R_w or R_s and *PGV*, H_L or γ_{max}, *PGV* showed basically the positive correlation in a certain range. With respect to the sites with high H_L, the ground motions reached the limit value and the damage by the ground motion were saturated. The results suggest that the depth of liquefied layer is a better factor when compared to H_L. The results of γ_{max} suggest that the ground deformation by liquefaction in upper layers directly causes pipe damage and the liquefaction in lower layers also causes the half degree of damage.

4) The fragility curves were modeled by classifying target sites based on *PL*-value considering ground conditions. The damage ratio of the sites with $PL \geq 15$ rose at approximately a 0.10 m/s lower *PGV* when compared with that for $PL < 15$. The result suggests that it is possible to underestimate the damage ratio with the fragility curve that does not include the *PL*-value information.

6. ACKNOWLEDGMENTS

The authors greatly appreciate the thoughtful comments and suggestions by Liquefaction Countermeasure Committee in Kamisu City (Chairperson: Professor Susumu Yasuda at Tokyo Denki University) and all the associated members in the committee. In this study, we would like to deeply appreciate the use of strong motion records offered by National Research Institute for Earth Science and

Disaster Resilience.

7. REFERENCES

The Water Supply Division, Health Service Bureau, Ministry of Health, Labour and Welfare (MHLW). 2013. Final report of Damage of water facilities due to Great East Japan Earthquake, March 2013 (In Japanese) http://www.mhlw.go.jp/topics/bukyoku/kenkou/suido/houkoku/suidou/130801-1.html (accessed 2018.3.5).

Sewerage Technological Examination Committee for Earthquake and Tsunami. Final report, March 2016 (In Japanese) http://www.mlit.go.jp/mizukokudo/sewerage/crd_sewerage_tk_000170-1.html (accessed 2018.3.5).

Hwang, HMH, Lin, H, Shinozuka, M (1998). Seismic performance assessment of water delivery systems. *Journal of Infrastructure Systems*, 4(3): 118-125.

Liu, GY, Hung, HY (2009). Seismic performance simulation of water systems considering uncertainties in ground motions and pipeline damages. *Safety, Reliability and Risk of Structures, Infrastructures and Engineering Systems,* Taylor & Francis, London: 2316-2321.

Javanbarg, MB, Takada, S (2009). Seismic reliability assessment of water supply systems. *Safety, Reliability and Risk of Structures, Infrastructures and Engineering Systems,* Taylor & Francis, London: 3455-3462.

Shoji, G, Naba, S, Nagata, S (2011). Evaluation of Seismic Vulnerability of Sewerage Pipelines based on Assessment of the damage data in the 1995 Kobe Earthquake, Applications of Statistics and Probability in Civil Engineering eds by M. H. Faber, J. Kőhler and K. Nishijima, Taylor & Francis, London: 1415-1423.

Naba, S, Tsukiji, T, Shoji, G, Nagata, S (2012). Damage assessment on water supply system and sewerage system at the 2011 off the Pacific Coast of Tohoku Earthquake -Case study for the data at Ibaraki and Chiba prefectures-. *Proceedings of the International Symposium on Engineering Lessons Learned from the 2011 Great East Japan Earthquake*, Tokyo, 1-4 March 2012, pp 1487-1495.

Toprak, S, Nacaroglu, E, Koc, AC, van Ballegooy, S, Jacka, M, Torvelainen, E, O'Rourke, TD (2017). Pipeline damage predictions in liquefaction zone using LNS. *Proceeding 16th World Conference on Earthquake,* 16WCEE 2017, Santiago Chile, 9-13 January 2017, Paper N° 4533.

Tsukiji, T and Shoji, G (2013). Development of Damage Functions on Water Supply Systems subjected to an Extreme Ground Motion, Proceedings of the 11th International Conference on Structural Safety and Reliability (ICOSSAR2013), New York, USA, Safety, Reliability, Risk and Life-Cycle Performance of Structures & Infrastructures eds by G. Deodatis, B. R. Ellingwood and D. M. Frangopol, CRC Press Taylor & Francis, London, pp 691-698.

Unjoh, S, Kaneko, M, Kataoka, S, Nagaya, K, Matsuoka, K (2013). Effect of earthquake ground motions on soil liquefaction. *Soils and Foundations,* 52(5):830-841.

Yoshida, N, Towhata, I (1991). YUSAYUSA-2 and SIMMDL-2, Theory and Practice, revised in 2003 (Version 2.10) http://www.kiso.co.jp/yoshida/ (accessed 2018.3.5).

The Kanto District Bureau of Ministry of Land, Infrastructure, Transport and Tourism (MILT) (2011). Survey Results of Soil Liquefaction in Kanto region at the 2011 off the Pacific Coast of Tohoku earthquake and tsunami. (In Japanese) http://www.ktr.mlit.go.jp/ktr_content/content/000043569.pdf (accessed 2018.3.5).

Japan Road Association (JRA) (2012). Bridge Design Specifications, Part V Seismic Design (In Japanese).

Hatanaka, M, Uchida, A (1996). Empirical correlation between penetration resistance and internal friction angle for sandy soils, *Soils and Foundations*, 36(4): 1-9.

Creager, WP, Justin, JD, Hinds, J (1945). *Engineering for Dams*, Vol. III, Earth, Rock-fill, Steel and Timber dams, John Wiley & Sons, Inc., N.Y., pp 645-649.

Ishihara, K, Towhata, I (1980). One-Dimensional Soil Response Analysis during Earthquakes Based on Effective Stress Method, *Journal of Faculty of Engineering*, XXXV(4): 655-700.

National Research Institute for Earth Science and Disaster Prevention (NIED) 2011. *K-NET and KiK-net.* (In Japanese) http://www.kyoshin.bosai.go.jp/kyoshin/ (accessed 2018.3.5).

Yoshida N, Suetomi I (1996). DYNEQ: a computer program for dynamic analysis of level ground based on equivalent linear method. Reports of Engineering Research Institute, Sato Kogyo Co., Ltd, pp 61-70 (In Japanese).

Architectural Institute of Japan (1988). Recommendations foe Design of Building Foundations, pp.163-169 (In Japanese).

Iwasaki, T, Tatsuoka, H, Tokida, K, Yasuda, S (1980). Estimation of degree of soil liquefaction during earthquake. *Soils and Foundations (Tsuchi-to-Kiso)*, 28(4): 23-29 (In Japanese).

Japan Meteorological Agency (JMA) (2011). Data of seismic intensity by local public organization. http://www.data.jma.go.jp/svd/eqev/data/kyoshin/jishin/110311_tohokuchiho-taiheiyouoki/index2.html (accessed 2018.3.5).

Sakurai, T, Shoji, G, Takahashi, K, Nakamura, T (2012). Damage assessment on road structures due to slope failures in the 2011 off the Pacific Coast of Tohoku earthquake. *Proceedings of the International Symposium on Engineering Lessons Learned from the 2011 Great East Japan Earthquake*, Tokyo, 1-4 March 2012, pp 961-972.